Discussion of the Axial Ratio of a Square Loop Antenna with an Attenuating Current

Hisamatsu Nakano, *Life Fellow*, *IEEE*, Tomoki Abe, *Member*, *IEEE*, Amit Mehta, *Senior Member*, *IEEE*, Junji Yamauchi, *Life Fellow*, *IEEE*

***Abstract*—The quality of the radiation field from a square loop antenna is evaluated using ARz, the axial ratio on the z-axis normal to the loop plane. For this evaluation, a generalized antenna model is used, where the current on a loop that is one guided wavelength in length is assumed to travel only in the forward direction, without backward currents. Firstly, the radiation field is formulated for the situation where the traveling wave current decays with attenuation constant α. It is found that ARz exponentially degrades as α increases. Secondly, a reactive current of weight q is superimposed onto the original current used for the first derivation. It is revealed that the degraded ARz is remarkably improved by the superimposed current. Throughout this discussion the difference in the axial ratios of the square and round loop antenna models is clarified.**

***Index Terms*—axial ratio, circularly polarized radiation, square loop.**

I. INTRODUCTION

Antennas that radiate a circularly polarized (CP) wave typically have either a round shape or a square shape [1]-[10]. Figures 1(a) and (b) depict, respectively, natural and metamaterial loop antennas, both having a square shape. These are the counterparts of the round loop antennas in [11].

The radiation from the square loop antennas in Fig. 1 is generated by the current that flows from feed point *F* to arm end point *T*, where a matched load is attached [12]. When the loop peripheral length is chosen to be one-guided wavelength ($1\lambda_g$) of the current, the phase for a pair of current elements located at points symmetric with respect to the center point of the loop become spatially in-phase. These generate strong radiation on the antenna axis (the z-axis, normal to the antenna plane), that rotates with time. As a result, the loop antennas in Fig. 1 operate as CP antennas.

The quality of the radiation field for CP antennas is evaluated using the axial ratio (AR) [13][14]. It is known that the AR for a non-resonant CP antenna, whose radiation is generated by a traveling wave current on the antenna conductor, is degraded by backward currents (currents reflected toward the feed point). Recently, an additional cause of AR degradation has been discussed using a generalized *round* loop antenna model [11], where the current on a loop of $1\lambda_g$ circumference decays with attenuation constant α due to radiation. The discussion in [11] leads to the conclusion that the AR on the antenna axis is degraded by the attenuation of the traveling wave current, even when backward currents do not exist.

The above discussion raises new academic questions: (1) Does attenuation of the current on the *square* loop antennas in Fig. 1 affect the AR? (2) If so, how does the AR of the square loop antennas behave? (3) Are there any remarkable differences in the AR behaviors between square and round loop antennas? (4) Is it possible to mitigate the degradation of the AR? To the best of our knowledge, answers to these questions have not yet been reported.

In this context, this letter presents answers to the above questions, using the generalized square loop antenna model shown in Fig. 2.

Five sections constitute this paper. After this introduction (section I), the radiation field generated by a forward traveling wave current on the loop is formulated in section II. Based on the formulated radiation field, the axial ratio on the antenna axis, ARz, is derived in section III. This is compared to the axial ratio of the corresponding round loop antenna model, ARs [11]. It is clarified how ARz behaves differently from ARs. In section IV, a reactive current is superimposed onto the original current in section II and the axial ratio in this situation is denoted as ARzq. We investigate whether this superimposition is effective in mitigating the degradation of ARz. Section V summarizes the findings of this research.

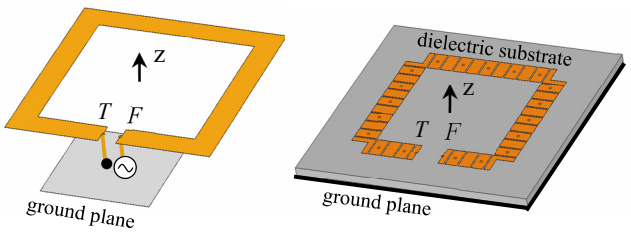

Fig. 1. Square loop antennas, where *F* is the feed point and *T* is the arm end with a matched load. (a) Natural square loop antenna. (b) Metamaterial square loop antenna (Metaloop antenna).

Manuscript received xxxxx 2023; revised xxxxx; accepted xxxxx. Date of publication xxxxx; date of current version xxxxx.

[1)]H. Nakano, [2)]T. Abe, and [3)]J. Yamauchi are all with the Department of Science and Engineering, Hosei university, Tokyo 184-8584, Japan (e-mail: [1)]hymat@hosei.ac.jp, [2)]tomoki.abe.5r@gmail.com, and [3)]j.yma@hosei.ac.jp). A. Mehta is with the Department of Science and Engineering, Swansea University, Bay Campus, Fabian Way, Swansea, SA1 8EN, UK (e-mail: a.mehta@swan.ac.uk)

Color version of one or more of the figures in this paper are available online at xxxx.

Digital Object Identifier xxxx

II. Radiation

Point F and end point T in the generalized square antenna model in Fig. 2 are separated by an infinitesimal space that is treated as zero in the following derivation. The peripheral length of the antenna model, C_{loop}, is chosen to be one guided wavelength of the current on the loop, such that the maximum radiation appears on the z-axis: $C_{\text{loop}} = 8l = 1\lambda_g$, with side length $2l = \lambda_g/4$ at frequency f.

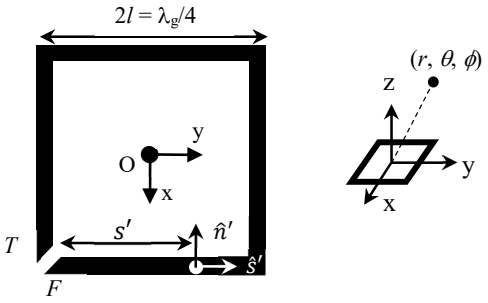

Fig. 2. Generalized square loop antenna model. It is assumed that the current on the loop travels only in the forward direction without backward currents. The forward current has attenuation constant α.

We express a forward traveling wave current on the loop as

$$\boldsymbol{I}(s') = I_0 e^{-(\alpha+j\beta)s'}\hat{s}' \tag{1}$$

where I_0 is the current value at point F; α and β ($= 2\pi/\lambda_g$) are the propagation attenuation and phase constants, respectively; and $\hat{s}'$ is the tangential unit vector at a point specified by length s'.

Note that the square loop antennas in [15] have been investigated without considering an attenuation constant. Hence, the effects on the radiation field of α (and hence the axial ratio, AR) have not been revealed.

The radiation field generated by current $\boldsymbol{I}(s')$ is calculated from the following equation [14].

$$\boldsymbol{E}(r,\theta,\phi) = \frac{-j\omega\mu}{4\pi}\frac{e^{-jk_0 r}}{r}\int_0^{8l}\boldsymbol{I}(s')\, e^{jk_0\hat{r}\cdot\boldsymbol{r}'}\, ds' \tag{2}$$

where (r,θ,ϕ) are the spherical coordinates specified by unit vectors $(\hat{r},\hat{\theta},\hat{\phi})$; ω is the angular frequency ($\omega = 2\pi f$); μ is the permeability; k_0 is the wave number in free space ($k_0 = 2\pi/\lambda_0$); and $\boldsymbol{r}'$ is the position vector from the coordinate origin to the point specified by length s'.

The current at the starting point of the m-th side arm (m = 1, 2, 3, 4), $s' = (2l)(m-1)$, is written as

$$I_0 e^{-(\alpha+j\beta)(2l)(m-1)}\hat{s}' \equiv I_0 c_m \hat{s}' \ (\text{m} = 1,2,3,4), \tag{3}$$

leading to $c_m = e^{-(\alpha+j\beta)(2l)(m-1)}$. The radiation field generated by the current on the first y-directed side arm, $\boldsymbol{e}_1(r,\theta,\phi)$, is calculated using Eq. (2).

$$\boldsymbol{e}_1(r,\theta,\phi) = C\int_0^{2l} c_1\,\hat{y}\, e^{-(\alpha+j\beta)s'}\cdot e^{jk_0\mathbf{r}_1'\cdot\hat{r}}\, ds' \tag{4}$$

where $C = -(j\omega\mu/4\pi)\cdot(e^{-jk_0 r}/r)\, I_0$; $\boldsymbol{r}_1'$ is the position vector from the coordinate origin to an arbitrary point on the first side arm; and

$$\mathbf{r}_1'\cdot\hat{r} = \sin\theta\{l\cos\phi + (s'-l)\sin\phi\}. \tag{5}$$

Note that vector $\hat{s}'$ in Eq. (1) is replaced by unit vector $\hat{y}$ in Eqs. (3) and (4) because of the direction of the first side arm.

Substituting Eq. (5) into Eq. (4), we obtain

$$\boldsymbol{e}_1(r,\theta,\phi) = C\int_0^{2l} c_1\,\hat{y}\, e^{-[\alpha+j\beta-jk_0\sin\theta\sin\phi]s'}\cdot e^{jM} ds'$$

$$= \hat{y}Cc_1\,\frac{e^{-(\alpha+j\beta)2l}e^{jP}-e^{jM}}{-\alpha-j\beta(1-\bar{k}\sin\phi)} \tag{6}$$

where the following notations are used:

$$P = k_0\, l\sin\theta(\cos\phi+\sin\phi) \tag{7}$$

$$M = k_0\, l\sin\theta(\cos\phi-\sin\phi) \tag{8}$$

$$\bar{k} = \frac{k_0}{\beta}\sin\theta \tag{9}$$

Similarly, the radiation fields from the remaining side arms for m = 2, 3, and 4 are derived as

$$\boldsymbol{e}_2(r,\theta,\phi) = -\hat{x}Cc_2\,\frac{e^{-(\alpha+j\beta)2l}\cdot e^{-jM}-e^{jP}}{-\alpha-j\beta(1+\bar{k}\cos\phi)} \tag{10}$$

$$\boldsymbol{e}_3(r,\theta,\phi) = -\hat{y}Cc_3\,\frac{e^{-(\alpha+j\beta)2l}\cdot e^{-jP}-e^{-jM}}{-\alpha-j\beta(1+\bar{k}\sin\phi)} \tag{11}$$

$$\boldsymbol{e}_4(r,\theta,\phi) = \hat{x}Cc_4\,\frac{e^{-(\alpha+j\beta)2l}\cdot e^{jM}-e^{-jP}}{-\alpha-j\beta(1-\bar{k}\cos\phi)} \tag{12}$$

The total radiation field is the sum of the radiation fields from the four side arms.

$$\mathbf{E}(r,\theta,\phi) = \sum_{\text{m}=1}^{4}\boldsymbol{e}_{\text{m}}(r,\theta,\phi) \tag{13}$$

The θ and ϕ components of Eq. (13) are

$$E_\theta(r,\theta,\phi) = \mathbf{E}(r,\theta,\phi)\cdot\hat{\theta} \tag{14}$$

$$E_\phi(r,\theta,\phi) = \mathbf{E}(r,\theta,\phi)\cdot\hat{\phi} \tag{15}$$

III. Axial Ratio

Square loop antennas of $1\lambda_g$ peripheral length have a wide radiation pattern. This means that the AR near the z-axis does not change remarkably from the AR on the z-axis ($\theta = 0$). Hence, understanding the behavior of the AR on the z-axis, ARz, contributes to evaluating the quality of the radiation field.

Using Eq. (13), the radiation field on the z-axis ($\theta = 0$) is derived using (P, M, $\bar{k}$) = (0, 0, 0).

$$\mathbf{E}(r, \theta = 0, \phi) = C\,\frac{e^{-(\alpha+j\beta)2l}-1}{-\alpha-j\beta}[\hat{y}(c_1 - c_3) + \hat{x}(-c_2 + c_4)]. \quad (16)$$

Because $C_{\text{loop}} = 8l = 1\lambda_g$, c_m(m = 1, 2, 3, 4) for $\beta > 0$ in Eq. (3) are

$$(c_1,\ c_2,\ c_3,\ c_4) = (1, -je^{-2l\alpha}, -1e^{-4l\alpha}, +je^{-6l\alpha}). \quad (17)$$

Hence, Eq. (16) yields

$$\mathbf{E}(r, \theta = 0, \phi) = C\,\frac{-je^{-2l\alpha}-1}{-\alpha-j\beta}(1 + e^{-4l\alpha})(\hat{y} + je^{-2l\alpha}\hat{x}). \quad (18)$$

The resulting field components are

$$E_\theta(r, \theta = 0, \phi) = C\,\frac{-je^{-2l\alpha}-1}{-\alpha-j\beta}(1 + e^{-4l\alpha})(\sin\phi + j\,e^{-2l\alpha}\cos\phi), \quad (19)$$

$$E_\phi(r, \theta = 0, \phi) = C\,\frac{-je^{-2l\alpha}-1}{-\alpha-j\beta}(1 + e^{-4l\alpha})(\cos\phi - j\,e^{-2l\alpha}\sin\phi). \quad (20)$$

Subsequently, we decompose the obtained field, $\mathbf{E}(r, \theta = 0, \phi)$, into the left-hand (LH) and right-hand (RH) CP components. The former and the latter are specified by L and R, respectively.

$$\mathbf{E}(r, \theta = 0, \phi) = E_\theta(r, \theta = 0, \phi)\hat{\theta} + E_\phi(r, \theta = 0, \phi)\hat{\phi} \equiv L(\hat{\theta} + j\hat{\phi}) + R(\hat{\theta} - j\hat{\phi}). \quad (21)$$

The components of L and R are

$$L = C\,\frac{-je^{-2l\alpha}-1}{2(-\alpha-j\beta)}(1 + e^{-4l\alpha})(1 - e^{-2l\alpha})(-je^{+j\phi}), \quad (22)$$

$$R = C\,\frac{-je^{-2l\alpha}-1}{2(-\alpha-j\beta)}(1 + e^{-4l\alpha})(1 + e^{-2l\alpha})(+je^{-j\phi}). \quad (23)$$

Using Eqs. (22) and (23), the axial ratio on the z-axis is derived:

$$\text{ARz} = \frac{|R|+|L|}{|(|R|-|L|)|} = e^{+2l\alpha}. \quad (24)$$

For comparison, the corresponding axial ratio for the generalized *round* loop antenna model, ARs, is quoted here [11]

$$\text{ARs} = \frac{\sqrt{\tilde{\alpha}^2+4}+\tilde{\alpha}}{\sqrt{\tilde{\alpha}^2+4}-\tilde{\alpha}}, \quad (25)$$

where $\tilde{\alpha} = a\alpha$, with a being the round loop radius and α being the attenuation constant of the forward traveling wave current. It is found that both axial ratios become the same only when $\alpha = 0$, i.e., the current has no attenuation. However, when $\alpha \neq 0$, Eq. (24) behaves differently from Eq. (25): the ARz can be represented by an exponential function.

Fig. 3 depicts Eq. (24) together with Eq. (25) as a function of attenuation constant α. Since $C_{\text{loop}} = 1\lambda_g$, a value of $l = \lambda_g/8 = 1/8$ is used for Eq. (24) and a value of $a = \lambda_g/2\pi = 1/2\pi$ is used for Eq. (25), both with $\lambda_g = 1$. It is found that the AR for the square loop antenna model degrades more than the AR for the round loop antenna model at the same α. Note that this is an inherent characteristic resulting from the square loop shape, not due to reflected currents (backward currents) generated at the loop corners, because we start with Eq. (1), which assumes that the current travels only in the forward direction. Also note that the red circles in Fig. 3 show the simulated axial ratios using the **E** resulting from the direct numerical integral of Eq. (1) in Eq. (2).

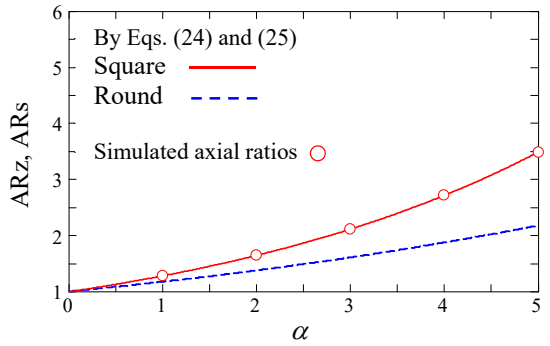

Fig. 3. Axial ratio as a function of attenuation constant α. The red solid line and blue dotted line depict Eqs. (24) and (25), respectively. The red circles show the simulated axial ratios.

IV. Mitigation of ARz Degradation

It is noted that a technique for mitigating the degraded AR for the round loop antenna (ARs) has already been discussed in [11], where a current is superimposed onto the original $\hat{s}'$-directed current. In this subsection, we apply a similar technique to the square loop antenna model and investigate whether the technique is effective.

The investigation starts with modification of Eq. (1) into Eq. (26), where the second term, specified by a reactive current of jqI_0 with $0 \le q \le 1$, is superimposed onto the original $\hat{s}'$-directed current.

$$\boldsymbol{I}(s') = I_0 e^{-(\alpha+j\beta)s'}\hat{s}' - jqI_0 e^{-(\alpha+j\beta)s'}\hat{n}' \quad (26)$$

where $\hat{n}'$ is the unit vector normal to the side arms, as shown in Fig. 2.

The original radiation field from the first side arm, Eq. (6), is modified into

$$\boldsymbol{e}_1(r,\theta,\phi) = (\hat{y} + jq\hat{x})Cc_1 \frac{e^{-(\alpha+j\beta)2l}e^{jP} - e^{jM}}{-\alpha - j\beta(1-\bar{k}\sin\phi)} \tag{27}$$

where $\hat{n}'$ is replaced by $-\hat{x}$.

Similarly, $\boldsymbol{e}_2(r,\theta,\phi)$ in Eq. (10), $\boldsymbol{e}_3(r,\theta,\phi)$ in Eq. (11), and $\boldsymbol{e}_4(r,\theta,\phi)$ in (12) are modified into

$$\boldsymbol{e}_2(r,\theta,\phi) = (-\hat{x} + jq\hat{y})Cc_2 \frac{e^{-(a+j\beta)2l}\cdot e^{-jM} - e^{jP}}{-\alpha - j\beta(1+j\bar{k}\cos\phi)} \tag{28}$$

$$\boldsymbol{e}_3(r,\theta,\phi) = (-\hat{y} - jq\hat{x})Cc_3 \frac{e^{-(a+j\beta)2l}\cdot e^{-jP} - e^{-jM}}{-\alpha - j\beta(1+\bar{k}\sin\phi)} \tag{29}$$

$$\boldsymbol{e}_4(r,\theta,\phi) = (\hat{x} - jq\hat{y})Cc_4 \frac{e^{-(a+j\beta)2l}\cdot e^{jM} - e^{-jP}}{-\alpha - j\beta(1-\bar{k}\cos\phi)} \tag{30}$$

The total radiation field, $\mathbf{E}(r,\theta,\phi)$, is the sum of Eqs. (27) through (30). On the antenna axis ($\theta = 0$), we have

$$\mathbf{E}(r,\theta=0,\phi) = C\frac{-je^{-2l\alpha}-1}{-\alpha-j\beta}(1+e^{-4l\alpha})$$
$$[(1+qe^{-2l\alpha})\hat{y} + j(q+e^{-2l\alpha})\hat{x}] \tag{31}$$

The field components of Eq. (31) are

$$E_\theta(r,\theta=0,\phi)$$
$$= C\frac{-je^{-2l\alpha}-1}{-\alpha-j\beta}(1+e^{-4l\alpha})\{(1+qe^{-2l\alpha})\sin\phi + j(q+e^{-2l\alpha})\cos\phi\} \tag{32}$$

$$E_\phi(r,\theta=0,\phi)$$
$$= C\frac{-je^{-2l\alpha}-1}{-\alpha-j\beta}(1+e^{-4l\alpha})\{(1+qe^{-2l\alpha})\cos\phi - j(q+e^{-2l\alpha})\sin\phi\} \tag{33}$$

Based on Eqs. (32) and (33), the LH CP and RH CP components of Eq. (31) are

$$L = -C\frac{-je^{-2l\alpha}-1}{2(-\alpha-j\beta)}(1+e^{-4l\alpha})(1-q)(1-e^{-2l\alpha})(je^{+j\phi}) \tag{34}$$

$$R = C\frac{-je^{-2l\alpha}-1}{2(-\alpha-j\beta)}(1+e^{-4l\alpha})(1+q)(1+e^{-2l\alpha})(je^{-j\phi}) \tag{35}$$

Using Eqs. (34) and (35), the axial ratio ARz of Eq. (24) is modified into a new axial ratio, denoted as ARzq, resulting from the superimposed $\hat{n}'$-directed current in Eq. (26).

$$\text{ARzq} = \frac{1+qe^{-2l\alpha}}{q+e^{-2l\alpha}} \tag{36}$$

The above equation leads to perfect CP radiation (ARzq = 1) when $\alpha = 0$. However, the value of $\alpha = 0$ is not realistic, because the traveling wave current attenuates due to the radiation. Fig. 4 illustrates ARzq. Again, a value of $l = \lambda_g/8 = 1/8$ with $\lambda_g = 1$ is used for $C_{\text{loop}} = 1\lambda_g$, as in Fig. 3. It is found that the degraded axial ratio ARz is improved in the presence of q ($q \neq 0$). Although not shown in this letter due to the page limit, this fact is confirmed by simulation. It follows that the current-superposition technique is effective for mitigating the degradation in the axial ratio. Note that some small circles plotted in Fig. 4 are the simulated axial ratios obtained using radiation field **E** that results from the direct numerical integral of Eq. (26) in Eq. (2).

For comparison, ARst in [11] is quoted here, which is the modified version of ARs of Eq. (25), resulting from the superimposed $\hat{t}'$-directed current on the corresponding round loop antenna model.

$$\text{ARst} = \frac{(1+p)\sqrt{\tilde{a}^2+4}+(1-p)\tilde{a}}{(1+p)\sqrt{\tilde{a}^2+4}-(1-p)\tilde{a}}\,. \tag{37}$$

where $\tilde{a} = a\alpha$, with a being the loop radius, as already mentioned in Eq. (25). It is found that the axial ratios ARzq and ARst differently behave except for a case of (q, p) = (1,1).

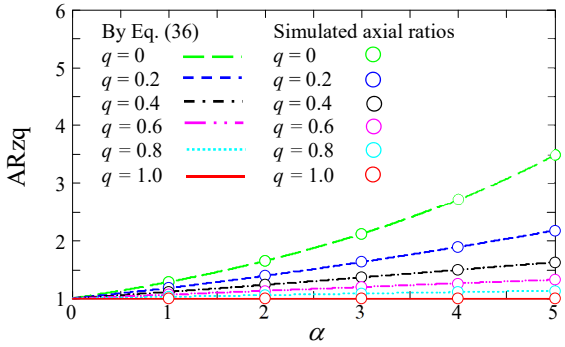

Fig. 4. ARzq as a function of attenuation constant α with q as a parameter. A value of $l = \lambda_g/8 = 1/8$ with $\lambda_g = 1$ is used for $C_{\text{loop}} = 1\lambda_g$. The circles show the simulated axial ratios.

V. Conclusions

The behavior of the axial ratio for square loop antennas has been discussed using a generalized loop antenna model of $1\lambda_g$ peripheral length, where a forward traveling wave current with attenuation constant α is assumed to flow on the loop. To clarify the effect of α on the axial ratio, it is also assumed that no reflected currents (backward currents) exist. It is found that the axial ratio, denoted as ARz, *exponentially* increases as α increases, unlike the axial ratio of the corresponding generalized round loop antenna model, denoted as ARs. Subsequently, a reactive current of weight q is superimposed onto the original current for the square loop antenna. The axial ratio in this case, denoted as ARzq, is found to be different from the ARst (the axial ratio for the corresponding round loop antenna model). It is also found that the reactive current superimposition is effective in mitigating the AR degradation due to an attenuating current.

REFERENCES

[1] Z. Chen, D. Liu, H. Nakano, X. Qing, *Handbook of Antenna Technologies*, Springer, 2016.

[2] C. Balanis, *Antenna Theory, analysis and design*, 3rd ed. Wiley, Hoboken, NJ, 2005.

[3] H. Nakano, K. Yoshida, and J. Yamauchi, "Radiation characteristics of a metaloop antenna," IEEE Antennas and Wireless Propagation Letters, vol. 12, pp. 861-863, June 2013.

[4] J. A. Kaiser, "The Archimedean two-wire spiral antenna," IRE Transactions on Antennas and Propagation, vol. AP-8, pp. 312-323, May 1960.

[5] H. Nakano, K. Nogami, S. Arai, H. Mimaki, and J. Yamauchi, "A spiral antenna backed by a conducting plane reflector," IEEE Transactions on Antennas and Propagation, vol. AP-34, pp. 791-796, 1986.

[6] H. Nakano, J. Miyake, M. Oyama, and J. Yamauchi, "Metamaterial spiral antenna," IEEE Antennas and Wireless Propagation Letters, vol. 10, pp. 1555-1558, 2011.

[7] J. Kraus, R. Marhefka, *Antennas*, 3rd edition, McGraw Hill, NY, 2002.

[8] H. Nakano, *Low-Profile Natural and Metamaterial Antennas: Analysis Methods and Applications,* Wiley-IEEE Press, NY, 2016.

[9] L. Shafai, "Some array applications of the curl antenna," Electromagnetics, vol. 20, no. 4, pp. 271-293, July 2000.

[10] H. Nakano, S. Okuzawa, K. Ohishi, M. Mimaki, and J. Yamauchi, "A curl antenna," IEEE Transactions on Antennas and Propagation, vol. 41, no. 11, pp. 1570-1575, November 1993.

[11] H. Nakano, T. Abe, A. Mehta, and J. Yamauchi, "Theoretical consideration of axial ratio deterioration in CP loop-shaped antennas," IEEE Antennas and Wireless Propagation Letters, vol. 22, no.5, pp. 1035-1039, May 2023.

[12] R. Collin, *Foundations for microwave engineering*, Second ed. Wiley-IEEE Press, NY, 2001.

[13] J. Kraus and R. Marhefka, *Antennas*, 3rd ed. New York, NY, USA: McGraw-Hill, 2002.

[14] E. Yamashita, *Analysis Methods for Electromagnetic Wave Problems*. Norwood, MA, USA, Artech House, 1996.

[15] H. Nakano, T. Abe, and J. Yamauchi, "Phase progression of a radiation field from circular and square active regions," IEEE Access, vol. 9, pp. 14710-14724, Jan. 2021.